

Distributing quantum correlations through local operations and classical resources

Adam G. Hawkins,¹ Hannah McAleese,¹ and Mauro Paternostro^{2,1}

¹Centre for Quantum Materials and Technologies, School of Mathematics and Physics, Queen's University Belfast, BT7 1NN Belfast, UK

²Quantum Theory Group, Dipartimento di Fisica e Chimica - Emilio Segrè,
Università degli Studi di Palermo, via Archirafi 36, I-90123 Palermo, Italy

(Dated: December 9, 2024)

Distributing quantum correlations to each node of a network is a key aspect of quantum networking. Here, we present a robust, physically motivated protocol by which global quantum correlations, as characterized by the discord, can be distributed to quantum memories using a mixed state of information carriers which possesses only classical correlations. In addition, such distribution is done using only bilocal unitary operations and projective measurements, with the degree of discord being measurement-outcome independent. We explore the scaling of the performance of the proposed protocol with the size of the network and illustrate the structure of quantum correlations that are shared by the nodes, showing its dependence on the local operations performed. Finally, we find the counterintuitive result that even more discord can be generated when the resource state undergoes correlated dephasing noise, allowing high fidelities with mixtures of the Bell basis such as Werner states.

I. INTRODUCTION

In recent times, the idea of a quantum internet [1, 2] has become one of the most sought-after uses of quantum resources in modern quantum information theory. In particular, the leveraging of quantum entanglement as a resource to perform communication in a way that is not allowed in classical communication is paramount to gaining quantum advantage. Entanglement is often referred to by the blanket term “quantum correlations”, however, with the concept of quantum discord [3, 4], one can only consider entanglement to be a subset of what can be labelled as quantum (or “non-classical”) correlations. In fact, it is possible for states to possess non-zero quantum correlations while simultaneously exhibiting zero entanglement [5], and so measures of entanglement do not, in general, capture all of the quantum correlations of a given system.

The full usefulness of said states with regards to quantum information processing remains to be seen. However, it has been shown that a state with non-zero discord can always be used to ‘activate’ bipartite entanglement between a system and a corresponding auxiliary; hence, discord is a resource in quantum information processing [6]. For certain separable non-classical states, it has been shown that this entanglement can be localized to the original system via stochastic entanglement swapping [7]. Furthermore, it has been established that discord is a resource for a number of applications, such as quantum computation [8, 9], remote state preparation [10], state discrimination [11–14] and quantum cryptography [15, 16].

Just as with entanglement, if quantum discord is to be used as a resource in quantum networking, then methods for distributing it to quantum memories at each node of the network must be established. For entanglement to be distributed, either the entanglement can be generated initially to then be sent directly to the memories, or some sort of non-local operation(s) must be in-

troduced to the memories. However, it has been shown that it is possible to generate discord via *local*, non-unitary channels acting on one or more of the subsystems in a state [17–19], with multiple physical examples of said discord generation being detailed [20–22]. These discordant states often have asymmetric structures, depending on the channel which is applied. If discord is distributed to quantum memories in a network, the possibility of entanglement distribution to these discordant states via interactions with a *separable* carrier state then arises [23–26]. Thus, discord is a resource in entanglement distribution [27, 28].

Here, we take the idea of locally generating discord and outline a robust discord distribution protocol. This protocol involves a source of information carriers, which are initially in a mixed, classically correlated state, being used to distribute significant amounts of discord to spatially-separated quantum memories. This is done via local unitary interactions (with respect to the memories) and projective measurements only. We show here that this distribution of discord does not depend on the measurement outcomes of said projective measurements; only the basis used to measure the information carriers determines the amount of distributed discord. In fact, we detail a modified version of this protocol whereby a discordant resource state of a quantum key distribution (QKD) protocol can be generated with unit probability. Our protocol not only appears to scale well with the number of memories in the network, but also exhibits robustness to the preparation and measurement apparatus used. Moreover, we highlight how the protocol can perform even better under certain correlated noise models.

In Sec. II, we describe the bipartite protocol and describe the quantum channel acting on the memories as a result of the protocol, while also outlining different types of discordant states. We then investigate the robustness of the bipartite protocol in Sec. III with respect to measurement apparatus as well as the initial carrier and memory states. We further evaluate how our chosen

quantifier of the quantum correlations affects how much discord is present in the final state, while also seeking numerical evidence of the true resource of the protocol. In Sec. IV, we consider protocols involving more memories, and calculate how the amount of distributed discord scales with the number of nodes in the network. We also offer a benchmark to gauge how significant the amount of distributed discord is for each system size. In Sec. V, we explore the structure of the discordant final states of the memories upon the conclusion of the protocol, and how such structure depends on the local operations performed at each node. We consider and illustrate this for multiple system sizes in order to establish structural patterns and consistencies. We present our conclusions in Sec. VI and discuss potential future implementations of our protocol.

II. THE BIPARTITE PROTOCOL

Consider a source which outputs a pair of *carrier* qubits (labelled as C_1 and C_2 respectively) prepared in the mixed state

$$\rho_{C_1 C_2} = \frac{1}{2}(|++\rangle\langle++| + |--\rangle\langle--|)_{C_1 C_2}, \quad (1)$$

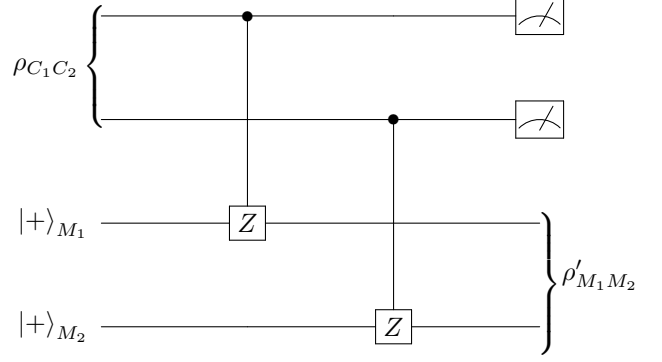
where $|\pm\rangle = (|0\rangle \pm |1\rangle)/\sqrt{2}$ is the eigenstate of the x Pauli operator with eigenvalue ± 1 , and $\{|0\rangle, |1\rangle\}$ is the computational basis of eigenstates of the z Pauli operator Z such that $Z|0\rangle = |0\rangle$ and $Z|1\rangle = -|1\rangle$. Eq. (1) obviously carries no quantum correlations. Each carrier is sent to a respective quantum memory, which we assume to be spatially separated by an arbitrary distance. The memories M_1 and M_2 are initially in the pure product state $\rho_{M_1 M_2} = |++\rangle\langle++|_{M_1 M_2}$.

A controlled- Z gate $U_{Z,i} = |0\rangle\langle 0|_{C_i} \otimes \mathbb{1}_{M_i} + |1\rangle\langle 1|_{C_i} \otimes Z_{M_i}$ is then performed over each carrier-memory pair $\{C_i, M_i\}$ ($i = 1, 2$), where $\mathbb{1}$ is the identity. The carriers are then locally measured in a suitable orthonormal basis $\{|\psi\rangle_{C_i}, |\psi^\perp\rangle_{C_i}\}$ with

$$|\psi\rangle_{C_i} = \cos \frac{\theta_i}{2} |0\rangle_{C_i} + e^{i\phi_i} \sin \frac{\theta_i}{2} |1\rangle_{C_i} \quad (2)$$

and ${}_i\langle\psi^\perp|\psi\rangle_{C_i} = 0$. We have introduced the Bloch angles $\theta_i \in [0, \pi]$ and $\phi_i \in [0, 2\pi)$ for the carrier C_i . Such simple protocol can be presented diagrammatically by

the following quantum circuit



where we have used the standard symbols for the U_Z gate. We are interested in the reduced state of the memories upon application of the protocol

$$\rho'_{M_1 M_2} = \mathcal{N} \text{Tr}_{C_1 C_2} \left[\Pi_\psi U_{CM} (\rho_{C_1 C_2} \otimes \rho_{M_1 M_2}) U_{CM}^\dagger \Pi_\psi \right] \quad (3)$$

with $U_{CM} = U_{Z,1} \otimes U_{Z,2}$, $\Pi_\psi = |\psi\rangle\langle\psi|_{C_1} \otimes |\psi\rangle\langle\psi|_{C_2}$ and \mathcal{N} denoting a normalization constant. We stress that we cannot interpret the evolved state of the memories as the output of individual quantum channels applied to M_1 and M_2 as the carriers are initially classically correlated. We do, however, highlight that the operations performed are *local* with respect to the $M_1 : M_2$ partition, i.e., the protocol is *bilocal*. The final reduced state of the memories takes the following form:

$$\rho'_{M_1 M_2} = \bigotimes_{i=1,2} \left(\cos^2 \frac{\theta_i}{2} |+\rangle\langle+| + \sin^2 \frac{\theta_i}{2} |-\rangle\langle-| \right)_{M_i} + \alpha(\theta_1, \theta_2) (e^{i\phi_+} |++\rangle\langle--| + e^{i\phi_-} |+-\rangle\langle-+| + \text{h.c.})_{M_1 M_2} \quad (4)$$

with $\alpha(\theta_1, \theta_2) = (\sin \theta_1 \sin \theta_2)/4$ and $\phi_\pm = \phi_1 \pm \phi_2$. For suitable choices of the parameters of the projections performed on the carriers, Eq. (4) might bring about quantum correlations. We include a brief analysis of this protocol – with respect to the quantum channel involved – as an appendix to this paper.

To quantify the quantum correlations, we choose the quantum discord in its original definition [3, 4]: Consider a bipartite quantum system prepared in state ρ_{AB} . We introduce the mutual information $I(A : B)$ – a measure of the total correlations within a given quantum state – and total classical correlations $J(A : B)$

$$I(A : B) = S(\rho_A) + S(\rho_B) - S(\rho_{AB}), \quad (5)$$

$$J(A : B) = S(\rho_A) - S(\rho_{A|B}), \quad (6)$$

where $S(\mu)$ is the von Neumann entropy of the generic state μ . Here, $\rho_{A(B)} = \text{Tr}_{B(A)}[\rho_{AB}]$ and $\rho_{A|B}$ are the reduced state of subsystem A (B) and the conditional state of A given a measurement performed on B , respectively. The measurement on B is modelled as a set of rank-1 projectors $\{\Pi_j^B\}$ [29] labelled by the index j of the corresponding measurement outcomes, each occurring with a probability $p_j = \text{Tr}[\Pi_j^B \rho_{AB}]$. The difference

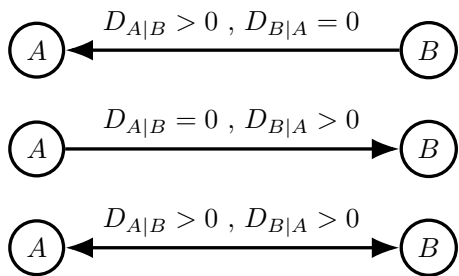


FIG. 1. Graphical representations of possible discord structures between two arbitrary systems A and B . In the bottom diagram, $D_{A|B}$ is not necessarily equal to $D_{B|A}$. We present *classical-quantum*, *quantum-classical*, and *quantum-quantum* states in a top-to-bottom configuration.

between $I(A : B)$ and $J(A : B)$, minimized over all the projective measurements on B , embodies the quantum discord [30]

$$D_{A|B} = S(\rho_B) - S(\rho_{AB}) + \min_{\{\Pi_j^B\}} \sum_j p_j S(\rho_{AB|\Pi_j^B}), \quad (7)$$

where $\rho_{AB|\Pi_j^B} = (\Pi_j^B \rho_{AB} \Pi_j^B) / p_j$ is the state resulting from the application of the measurement operators. A caveat of the above definition is that, in general, $D_{A|B} \neq D_{B|A}$ due to the asymmetric nature of the quantum conditional entropy [30]. In fact, there exist *classical-quantum* states, particularly those resulting from the action of local channels, which showcase $D_{A|B} > 0$ with $D_{B|A} = 0$ [7, 18]. Examples of such states include the resource state for the QKD protocol dubbed B92 [31] along with, in general, any state obtained as a result of the protocol proposed here but limited to just one quantum memory [32]. The different one- and two-way discord structures are shown graphically in Fig. 1.

When using Eq. (7), the maximum degree of discord in state (4) (obtained by optimizing with respect to the four angles entering it) is found to be $D_{M_1|M_2} \simeq 0.2018$ [33], which is also the maximum amount of locally generated discord achievable – starting with a classically correlated state – in a bipartite qubit system [18]. Such result can be achieved by picking up values for the angles θ_j and ϕ_j from a manifold, an interesting example being $\theta_1 = \pi/2$, $\theta_2 = \pi/4$, for any choice of $\phi_{1,2}$. While, needless to say, different choices of parameters taken from the optimal manifold would result in different (yet iso-discordant) states, such optimal degree of discord is obtained *independently* of the value of the relative phases ϕ_j chosen for the measurements on the carriers: All the memory states achieved by projecting the carriers onto the elements of a chosen measurement basis bring about the same degree of discord. In a sense, this implies that the protocol described here actually prepares states belonging to *subspaces* of iso-discordant states. Among such subspaces, there is one whose elements all achieve the degree of discord of the B92 resource state. In practical terms, the data achieved for

any detection configuration belonging to such optimal plane could be retained for the sake of distributing maximum discord, and unless a *specific* discordant state is desired.

A. Generating the Resource State for the B92 QKD Protocol

Finally, it is worth noting that this protocol may be rewritten in different bases for the purpose of obtaining different states. For example, by writing the protocol in the computational basis $\{|+\rangle, |-\rangle\} \rightarrow \{|0\rangle, |1\rangle\}$ and using a controlled-Hadamard gate instead of a controlled- Z , it is possible to achieve the discordant resource state of the B92 QKD protocol [31] with 100% probability. This is the case when only Bob's carrier C_2 interacts with M_2 (C_1 can either just be held by Alice or can be state-mapped onto M_1) and is then measured in any basis defined by $\theta_2 = \pi/2$ (e.g., $\{|+\rangle, |-\rangle\}$), with both measurement outcomes projecting the final state onto the B92 resource state; not only is the amount of discord independent of the measurement outcome but so is the state, which itself is not a function of ϕ_2 . This would mean that, instead of the method outlined in Ref. [34], the protocol can be performed in the case where the resource state is supplied to Alice and Bob by a trusted third party – without the need for any direct initial classical communication or exchanging of quantum states between themselves. The third party can help perform this protocol while also not knowing which of the pure states in the mixture have been supplied to Alice and Bob. If the third party is untrusted, though, then this method will no longer be secure, as they can know which pure state is supplied with certainty.

One may also consider extending this to an N -party conference key agreement (CKA) protocol which, in principle, could generate an identical key for 1 'Alice' and $N - 1$ 'Bob's (or vice versa). However, any such resource state, albeit discordant, would be completely separable, and it has been shown that any CKA protocol in which a single copy of a multipartite state is distributed to all parties involved requires (biseparable) entanglement to be unconditionally secure [35, 36]. Furthermore, the B92 protocol performed in this way will have no guarantee of security against adversarial attacks even in the bipartite scheme; if an adversary correctly measures one of the carrier qubits before the controlled-Hadamard interaction in the computational basis then they will know, with certainty, which bit that Alice receives and which quantum state that Bob receives. Therefore, additional methods would need to be considered in order to overcome these vulnerabilities.

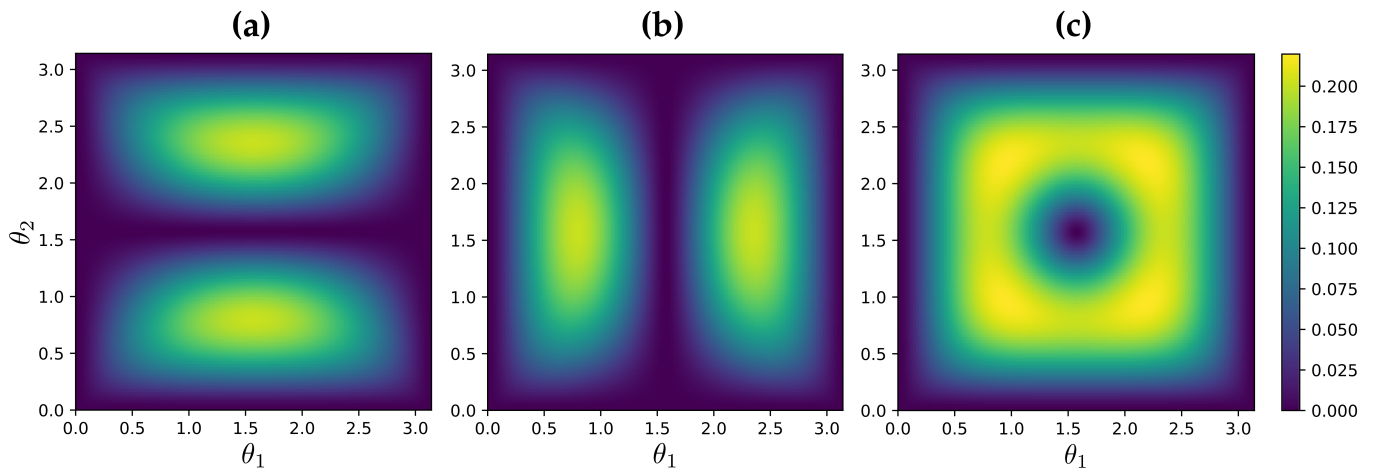


FIG. 2. Distributed quantum correlations in the state $\rho'_{M_1M_2}$ plotted against the parameters $\theta_{1,2}$ entering the measurements on the carriers. Since the amount of quantum correlations is independent of $\phi_{1,2}$, we set $\phi_1 = \phi_2 = 0$ without loss of generality. We consider three non-equivalent quantifiers of discord: panels (a) and (b) show the two asymmetric measures $D_{M_1|M_2}(\rho'_{M_1M_2})$ and $D_{M_2|M_1}(\rho'_{M_1M_2})$, respectively, while panel (c) is for the symmetric GQD $\mathcal{G}(\rho'_{M_1M_2})$.

III. ROBUSTNESS OF THE PROTOCOL

At this point, we introduce a different quantifier of quantum correlations, namely the *global quantum discord* (GQD) first defined in Ref. [37] so as to pave the way to and perform an analysis of the generated quantum correlations in protocols involving more than two memories (see Sec. IV). Quantitatively, GQD is defined as

$$\mathcal{G}(\rho_{\{X\}}) = \min_{\{\Pi_k\}} \left[S(\rho_{\{X\}} \parallel \Phi(\rho_{\{X\}})) - \sum_{j=1}^N S(\rho_{X_j} \parallel \Phi_j(\rho_{X_j})) \right], \quad (8)$$

where $\{X\} = \{X_1, \dots, X_N\}$ stands for the total system comprising each subsystem X_j , $S(\mu \parallel \tau)$ denotes the quantum relative entropy [38] between two generic states μ and τ , $\Phi_j(\rho_{\{X\}}) = \sum_{j'} \Pi_{j'}^{X_j} \rho_{X_j} \Pi_{j'}^{X_j}$ and $\Phi(\rho_{\{X\}}) = \sum_k \Pi_k \rho_{\{X\}} \Pi_k$, with $\Pi_k = \Pi_{j_1}^{X_1} \otimes \dots \otimes \Pi_{j_N}^{X_N}$ and k denoting the index string $(j_1 \dots j_N)$ [37]. Here, a projector is again represented by the symbol Π . Our choice of figure of merit is due to the fact that our interest when addressing a multipartite memory will move away from bipartitions to address the degree of quantum correlations shared by all the elements of the memory compound. Moreover, GQD bypasses the intrinsic asymmetry of Eq. (7), and we wish to explore how the distributed quantum correlations in the bipartite protocol differ depending on the quantifier. The maximum amount of GQD for the bipartite protocol of Sec. II is $\mathcal{G}_{M_1M_2} \simeq 0.2198$, which is achieved when both carriers are projected upon states belonging to “optimal subspaces” identified by $\theta_{1,2} = 0.9458, 2.1958$ and arbitrary values of $\phi_{1,2}$.

In the remainder of this Section, we will present a study of the robustness of the protocol valid for a bipartite memory system. We address the effect of imperfections at the preparation and measurement stages of the protocol, quantifying the influences on the degree of achieved quantum discord.

A. Measurement Precision

Firstly, we consider how the measurement basis of the carriers affects the final discord between the memories. In Figs. 2(a) and 2(b), we present the behavior of the two asymmetric discord definitions against $\theta_{1,2}$. In order to capture the quantum nature of all the quantum correlations, we also display our findings for the GQD in Fig. 2(c). This figure appears somewhat as a superposition of Figs. 2(a) and 2(b), though not adding together linearly. The maximum values of the asymmetric heatmaps are also apparent on the GQD one, although we see that higher GQD values are possible in some places where both asymmetric discords are non-zero. A further discussion to this can be found in Sec. V. Beside the edges of Fig. 2(c) – where, as discussed in the appendix, the distributed discord is null as the corresponding channel is both unital and semiclassical [17] – no quantum correlations are shared for $\theta_{1,2} = \pi/2$, for which the memories are left in the state $\rho_{M_1M_2} = (|00\rangle\langle 00| + |11\rangle\langle 11|)/2$.

From this analysis, it is clear that imprecise measurement settings would result in degrees of quantum discord that could be significantly different from the maximum achievable as illustrated previously. In order to evaluate such effects quantitatively, we assume the parameters $\theta_{1,2}$ defining the basis upon which a measurement of the carriers’ state should be performed to be

random variables – centred in the value that would allow us to achieve maximum discord – and varying uniformly within a range of a chosen width. As a figure of merit, we evaluate the average degree of discord achieved by letting the parameters vary. For an imprecision range as large as $\pi/10$, though, a reduction of the maximum degree of GQD of only 2% is achieved, thus demonstrating a good robustness of the protocol.

B. Initial State of the Carriers

Where the protocol is perhaps less robust, however, is with the initial state of the carriers. To investigate this, we consider the following convex combination of the desired carriers' state $\rho_{C_1C_2}$ and a state having no support on it, such as

$$\sigma(\lambda) = (1 - \lambda)\rho_{C_1C_2} + \frac{\lambda}{2}(|+-\rangle\langle+-| + |-+\rangle\langle-+|)_{C_1C_2} \quad (9)$$

with $\lambda \in [0, 1]$. We then consider the amount of GQD that is obtained if we measure the carriers in the optimal basis (for the ideal case) with different values of the mixing parameter for the initial carrier state. The results are presented in Fig. 3, where it can be seen that the amount of GQD between the memories is fairly sensitive to mixing parameter λ , and it reaches zero for $\lambda = 1$. We also calculate the average GQD distributed in the range $[0, 0.1]$ such that the robustness is tested in the case where the fidelity of the initial carriers cannot be guaranteed, which gives 0.1687: noticeably lower, yet still a significant amount of distributed GQD.

Remarkably, Fig 3 is identical to the graph obtained when maximising the GQD over $\theta_{1,2}$ at each value of λ , thus implying that the optimal bases for the ideal carrier state retain their optimality for all states defined as in Eq. (9). We investigate this further by generalising Eq. (9) to assume that the contributions of the $|++\rangle\langle++|$ and $|+-\rangle\langle+-|$ states in the mixture are not equal to the contributions of $|--\rangle\langle--|$ and $|-+\rangle\langle-+|$ states, respectively. Similarly, we find that less initial classical correlations results in a lower degree of GQD. However, when the initial carrier state $\frac{1}{2}(|+-\rangle\langle+-| + |-+\rangle\langle-+|)$ is used, the optimal amount of GQD generated is the same as when we use $\sigma(0)$ and for the same optimal carrier measurement basis. This shows the robustness of the protocol to phase flips of the carrier qubits.

To conclude this part of our analysis, we now assess the interplay between purity and classical correlations in the initial carrier state, which we take as

$$\rho_{C_1C_2}(\eta) = (\eta|++\rangle\langle++| + (1 - \eta)|--\rangle\langle--|)_{C_1C_2} \quad (10)$$

with $\eta \in [0, 1]$. Clearly, $\eta = 1/2$ corresponds to the state in Eq. (1), while increasing (decreasing) the parameter towards 1 (0) increases the purity of the state while simultaneously decreasing its classical correlations. Calculating the maximum possible distributed GQD as a

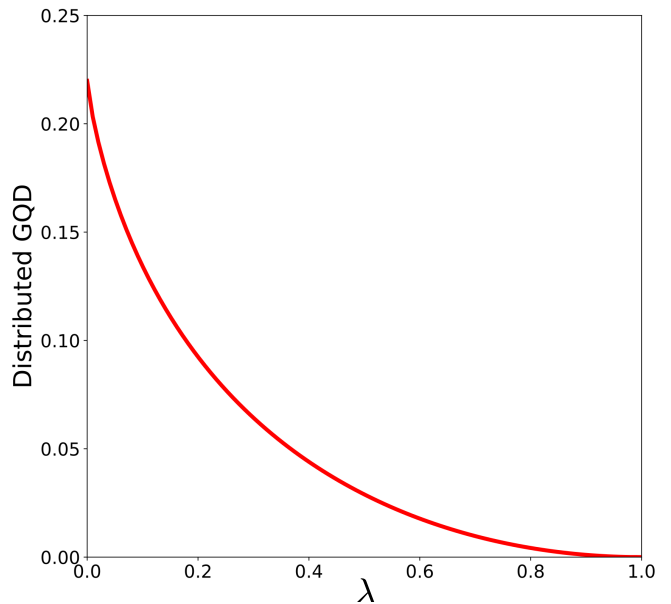


FIG. 3. A study of the bipartite GQD distributed to the memories against the mixing parameter λ in Eq. (9) and obtained assuming the optimal measurement bases for the carriers for any value of λ .

function of η , we find – quite expectedly – that as $\eta \rightarrow 0$ or 1, no GQD can be distributed. In general, GQD decreases as η deviates from 1/2 to disappear when such parameter takes its extremal values. This provides numerical evidence that classical correlations are the true resource of the protocol.

C. Initial State of the Memories

We now test the robustness of the protocol with respect to the initial state of the memories by considering two scenarios: pure states and mixed states. In the former, we consider the memories to be prepared in a pure product state, but where the fidelity of M_2 with $|+\rangle_{M_2}$ is non unit. In the latter, we consider the case where the initial state of both memories may have been subject to some level of noise, so that both memories are in mixed states.

We start considering the initial state of M_2

$$|\psi(\vartheta, \varphi)\rangle_{M_2} = \cos \frac{\vartheta}{2} |0\rangle + \sin \frac{\vartheta}{2} e^{i\varphi} |1\rangle. \quad (11)$$

where we have introduced the Bloch parameters $\vartheta \in [0, \pi]$ and $\varphi \in [0, 2\pi)$. We plot the GQD of the final state against ϑ and φ in Figs. 4(a) and 4(b). We do not change the measurement basis at this point and instead measure the carriers in the same basis which maximizes discord when $\rho_{M_1M_2} = |++\rangle\langle++|$. We find that, in analogy with the features highlighted previously on the carrier's measurement, the protocol is robust to any azimuthal phase

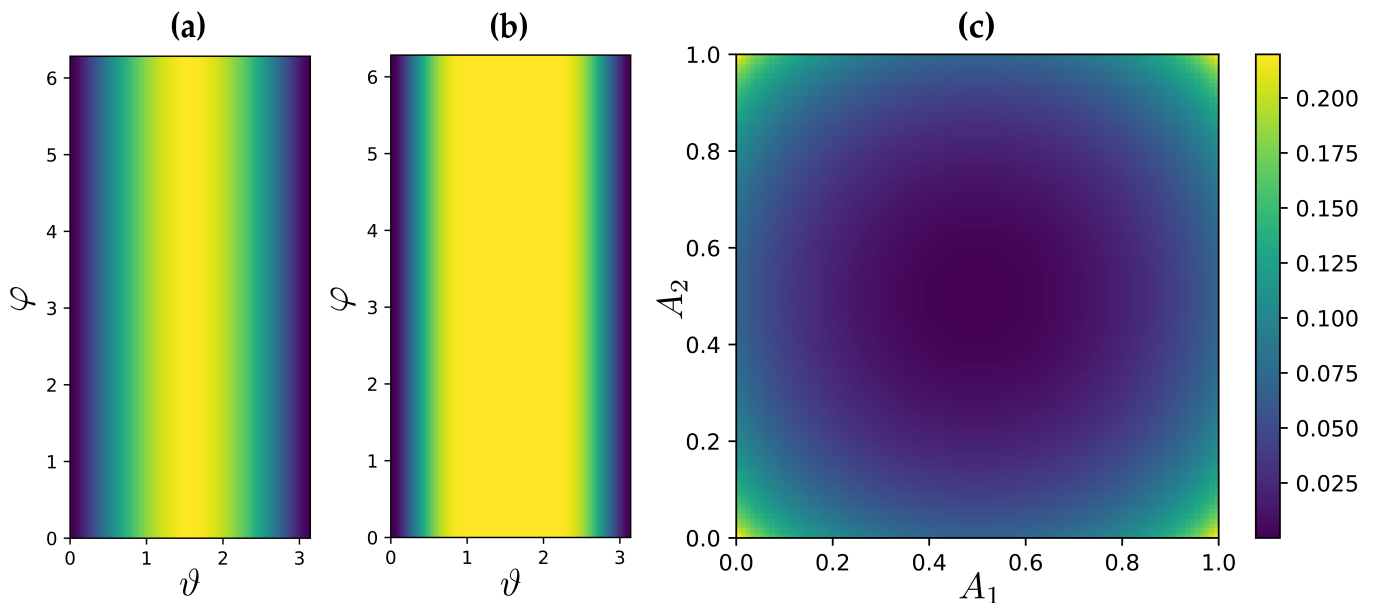


FIG. 4. The distributed GQD in the final M_1 - M_2 compound as a function of variables which define the initial state of memories. We first consider memories to be in a pure product state defined by ϑ and φ ; this is shown both for **(a)** the assumption that the carrier measurement bases used are characterized by $\theta_{1,2} = 0.9458$ and $\phi_1 = \phi_2 = 0$; and **(b)** optimization of the carrier measurements to show the largest amount of distributed GQD possible for each initial pure state of M_2 . Note that heatmap **(a)** will change depending on the value of ϕ_2 , but will always be at a maximum at $\vartheta = \pi/2$. In **(c)** we display the GQD in the final M_1 - M_2 compound as a function of the mixed-state parameters A_1 and A_2 , where we have again assumed $\theta_{1,2} = 0.9458$.

imprecision in the initial states of M_2 . GQD is maximized for $\vartheta = \pi/2$ and any choice for φ , so that states $| \pm \rangle$ and $| \pm i \rangle$ are all optimal. As noticed previously, GQD is weakly sensitive to small deviations from optimal initial states: for instance, the average GQD over a range symmetric around $\theta = \pi/2$ and of width $\pi/10$ (with $\phi_{1,2} = 0$) results in $\bar{G}_{M_1 M_2} = 0.2189$, which is a $\sim 0.4\%$ reduction with respect to the ideal value.

When a GQD value of 0.2198 is achievable, the change of each carrier measurement basis (in order to become optimal) depends only on the initial pure state of the memory with which each carrier interacts. That is, in Fig 4 **(b)**, only the measurement basis of C_2 need be adjusted in the range $0.96 \lesssim \vartheta \lesssim 2.18$. GQD here is, again, independent of the measurement outcome, however it does depend on the values of ϕ_2 that define the state upon which C_2 is projected. For the cases where a maximum GQD value of < 0.2198 is obtained in Fig 4 **(b)**, the optimal measurement basis for C_2 appears to be $\{ | +i \rangle, | -i \rangle \}$, meanwhile the optimal measurement basis for C_1 depends on the initial pure state of M_2 (again, not depending on the measurement outcome).

Let us now assume that both memories are initially in the following mixed state

$$\rho_{M_1 M_2}(A_1, A_2) = \bigotimes_{j=1,2} (A_j | + \rangle \langle + | + (1 - A_j) | - \rangle \langle - |)_{M_j} \quad (12)$$

with $A_j \in [0, 1]$. In Fig. 4**(c)** we plot the amount of GQD obtained when using an optimal photon basis against

$A_{1,2}$, confirming that GQD is maximized by preparing the memories in pure states, in line with the expectations stemming from the results reported in Figs. 4**(a)** and 4**(b)**. Again, Fig. 4**(c)** is identical to the case where we optimize over all carrier measurements for each plot point, solidifying the fact that the optimal bases are such not only in ideal conditions, but also for many non-ideal initial conditions that we consider in this paper. Thus, the maximum amount of GQD possible for a given initial state could be obtained without the need to change the measurement basis. The only counterexample we find in this paper is for some initial pure states of the memories with a fidelity of less than unity with $| + \rangle$ or $| - \rangle$, as shown in Fig. 4.

We include an assessment of the performance of the protocol when the memories experience correlated dephasing noise as an appendix to this manuscript, detailing instances in which the protocol can actually generate *more* quantum correlations as a result of such noise.

IV. ANALYSIS OF MULTIPARTITE MEMORY SYSTEMS

We now address systems of memory systems of a growing size, thus addressing explicitly the distribution of multipartite quantum discord. To such end, we start considering the same protocol as in Sec. II, but with N carriers and memories. The former are initially prepared

in

$$\rho_{\{C\}} = \frac{1}{2} (|+\dots+\rangle\langle+\dots+| + |-\dots-\rangle\langle-\dots-|)_{C_1 C_2 \dots C_N}, \quad (13)$$

where $\{C\}$ stands for the collection of N carrier systems. As for the memories, we assume them to be prepared in the N -party product state $\rho_{\{M\}} = |+\dots+\rangle_{M_1 M_2 \dots M_N}$. As in the bipartite case, each carrier C_j and memory M_j are subjected to a controlled- Z interaction, with the former being measured in a suitable basis to establish GQD between the memories. In Table I we report the distributed GQD for $N = 2, \dots, 5$ resulting from an extensive numerical search for the best possible performance. The values presented in Table I thus embody, at least, lower bounds to the maximum possible amount of distributed GQD to the memories [39]. We remark that, in line with the bipartite case, for $N \geq 3$ the same measurement basis will be needed for all the carriers, while the degree of distributed discord does not depend on the specific outcome of such measurements.

To provide a benchmark for the significance of the amount of distributed GQD for each system size, we also provide the amount of GQD present in the W state

$$|W_N\rangle = \frac{1}{\sqrt{N}} |N-1, 1\rangle, \quad (14)$$

where $|N-1, 1\rangle$ represents the totally symmetric state containing $N-1$ zeros and 1 one [40]. We stress that these states are not necessarily those with the largest amount of discord for each system size [41] – despite being maximally entangled – and serve only as a reference. Along with this, we consider the GQD of the Werner state $\rho_{W,N}$ for each N which has the same level of mixedness as the resulting state of the memories at the end of each protocol. We define $\rho_{W,N}$ as

$$\rho_{W,N}(\varepsilon) = (1-\varepsilon)|W_N\rangle\langle W_N| + \frac{\varepsilon}{2^N} \mathbb{1} \quad (\varepsilon \in [0, 1]). \quad (15)$$

N	\mathcal{G}_M	$\{\theta_i\}$	\mathcal{G}_W	\mathcal{G}_ε	$\mathcal{G}_M/\mathcal{G}_\varepsilon$
2	0.2198	0.9458	1.0000	0.4124	0.5330
3	0.4694	0.9131	1.5850	0.8070	0.5817
4	0.7040	0.8775	2.0000	1.1554	0.6093
5	0.9338	0.8533	2.3219	1.3749	0.6792

TABLE I. We report the values of $\mathcal{G}_M = \max_{\{\theta_i\}}[\mathcal{G}(\rho'_{\{M\}})]$, which represents a lower bound for the maximum amount of GQD possible in the final memory state $\rho'_{\{M\}}$. We also report the corresponding measurement parameters $\{\theta_i\}$ to identify exemplary optimal bases for all carriers to be measured in. In order to provide meaningful benchmarks, we display $\mathcal{G}_W = \mathcal{G}(|W_N\rangle\langle W_N|)$ and $\mathcal{G}_\varepsilon = \mathcal{G}(\rho_{W,N}(\varepsilon))$, the latter being the GQD of the state which has the same level of mixedness as each optimized $\rho'_{\{M\}}$. The ratios $\mathcal{G}_M/\mathcal{G}_\varepsilon$ give a simple figure of merit to track the scaling of the distributed GQD with the size of the system.

The ratio between the lower bound to the GQD of the memories achieved through our protocol and the corresponding quantity carried by the Werner state of the same degree of mixedness grows with N for all the cases numerically addressed here. Although we cannot confidently extrapolate a general behavior, this suggests that, not only does GQD increase with N , but also the amount of GQD with respect to allowed amount by system size improves. To give us an idea of the maximum amount of GQD for a given N , we use the few plot points we have to calculate the linear regression between the two: this gives us an approximate GQD of $0.238N - 0.250$ for N qubits. In Sec. V we put forward some arguments against the accuracy of such (intuitively reasonable) linear model.

To conclude this section, we briefly assess the performance of the protocol when it is performed using two carrier qubits which are in the tripartite GHZ state $\rho_{C_1 C_2 C_3} = |\text{GHZ}_3\rangle\langle\text{GHZ}_3|$, where $|\text{GHZ}_3\rangle = \frac{1}{\sqrt{2}}(|+++\rangle + |--\rangle)_{C_1 C_2 C_3}$. We do this since tracing out one of the carrier qubits from this state leaves the remaining two in the classically correlated state in Eq. (1). Assuming the protocol is performed for the memories M_1 and M_2 using carriers C_1 and C_2 , we verify that the maximum GQD in the final state of the compound M_1 - M_2 cannot be increased beyond the usual maximum, however a GQD increase from 1 (in the initial GHZ carrier state) to 1.2926 is possible for the state comprising M_1 - M_2 - C_3 . Any entanglement present in the state is lost when C_3 is traced out; this being true at any stage of the protocol.

V. DISCORD STRUCTURE OF THE FINAL STATE

We now conduct a deeper study of the discord structure of the prepared bipartite or multipartite discordant states. As we have already pointed out, the definition of discord in Eq. (7) is inherently asymmetric and, in fact, we have $D_{M_2|M_1} = 0$ when $D_{M_1|M_2}$ is maximized. On the other hand, it is interesting to analyze the state which achieves the maximum degree of GQD allowed by our protocol. As stated in Sec. III, this is achieved for carrier measurements with by $\theta_1 = \theta_2 = 0.9458$. A calculation of the degree of asymmetric discord for such state leads to $D_{M_1|M_2} = D_{M_1|M_2} = 0.1498$, showing the quantum-quantum nature of such resource and thus an inherently different sharing structure of quantum correlations within it than the one achieved by using the measurement settings maximizing $D_{M_1|M_2}$.

A similar line of thought can be pursued in the case of a multipartite system. We first consider the tripartite protocol, which we attack by implementing three different protocols, each identified by how many C_i - M_i compounds undergo controlled- Z interactions (followed by a measurement of C_i). For any C_i - M_i compound that does not experience such operations, we use C_i in the final state instead of M_i , which we trace out. We do

$\{i\}$ int.	12			23			13			123
	Cmpd.	$D_{1 2}$	$D_{2 1}$	Cmpd.	$D_{2 3}$	$D_{3 2}$	Cmpd.	$D_{1 3}$	$D_{3 1}$	Max. GQD
$\{1\}$	M_1C_2	✗	✓	C_2C_3	✗	✗	M_1C_3	✗	✓	0.2018
$\{1, 2\}$	M_1M_2	✓	✓	M_2C_3	✗	✓	M_1C_3	✗	✓	0.4036
$\{1, 2, 3\}$	M_1M_2	✓	✓	M_2M_3	✓	✓	M_1M_3	✓	✓	0.4694

TABLE II. Table displaying the discord structure of three different three-qubit discord distribution protocols, depending on which of the compounds (cmpds.) $\{C_i-M_i\}$ involve an interaction and measurement (int.). A ✗ indicates no discord is possible, meanwhile a ✓ indicates that the discord is non-zero in general (up to a maximum of 0.20175). Also displayed are the maximum possible values of the GQD of the total final state of each (assuming any measured carriers and unused memories are traced out). We note that the maximum GQD of the state with two interactions involved has a GQD which is exactly double the maximum asymmetric discord value of any resulting bipartite compound.

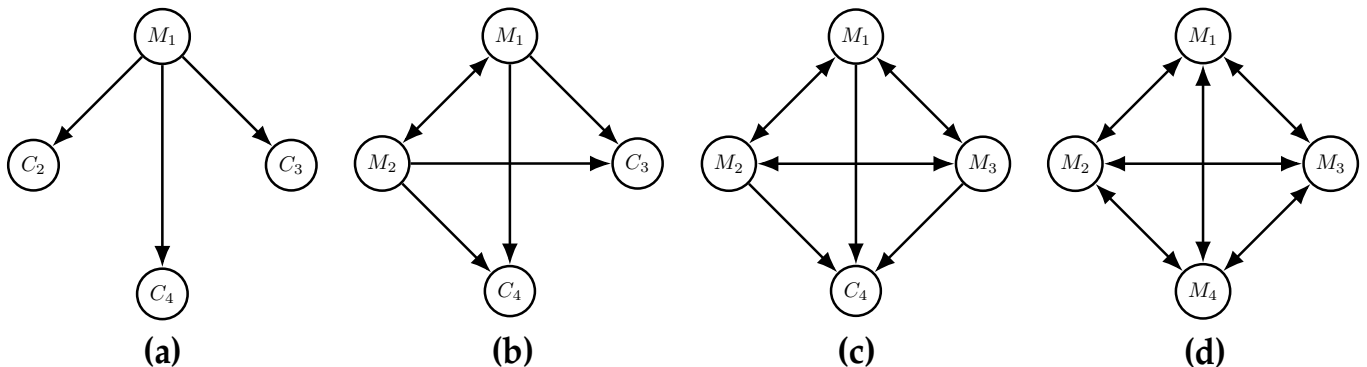


FIG. 5. Graphical representation of the discord structure of the final state of four differing discord distribution protocols with four qubits in the final state, based on the discord structure graphs shown in Fig. 1. These four protocols involve a growing number of interactions going from one to four (moving from panel (a) to (d)). All interactions occur between carriers and memories. Where an interaction (and measurement of carrier) takes place, a memory M_i is used in the final state with C_i being traced out. Where no interaction occurs, the unused memory is instead traced out in place of the carrier.

this so as to pin-point the dependence of both the structure and quantity of the quantum correlations on which local operations are performed. As the initial states of the system are invariant under particle exchange, we need not consider every permutation of operations performed, rather just the number of operations performed. Table II presents the results of our quantitative analysis.

We find that $D_{X_i|Y_j} = 0$ when $Y = C$ and $D_{X_i|Y_j} \neq 0$ when $Y = M$, for $X, Y \in \{C, M\}$ and $i \neq j$ are the labels identifying each carrier-memory compound ($i, j \in \{1, 2, 3\}$ for the tripartite protocol). Thus, if a carrier C_i interacts with a memory M_i before being measured, this, in general, creates asymmetric discord between M_i and the other states. Additionally, if, for $j \neq i$, the carrier C_j interacts with the memory M_j before being measured (and as long as the interaction happens before any other carrier measurements are made), this will also, in general, create asymmetric discord between M_j and M_i . Although, in general, discord is non-zero in both ‘directions’, we still call it asymmetric as $0 < D_{M_i|M_j} \neq D_{M_j|M_i} > 0$. To illustrate how this trend continues for higher-dimensional protocols more succinctly, we display the discord structure of the four possible ($N = 4$)-qubit protocols graphically in Fig. 5. Although we have not pursued this investigation further, we expect this trend to continue for all system sizes.

The maximum amount of asymmetric discord in any bipartite compound with non-zero discord is 0.2018, i.e. the same amount possible in the bipartite protocol. We see that, in the tripartite protocol, the maximum GQD in the resulting state when two sets of local operations occur is exactly double that value, meanwhile when all three involve local operations then it is slightly more than double. We find this pattern to similarly continue for the four qubit protocol: when three out of the four subsystems involve local operations, the maximum GQD is exactly triple the value of 0.2018, where again the maximum GQD when all memories are interacted with (and carriers are subsequently measured) is slightly more than triple. This suggests that the linear relation between the maximum GQD and the system size given earlier in this section could be replaced by the more accurate one

$$\mathcal{M}(N) = 0.2018(N - 1) + \xi(N), \quad (16)$$

where ξ is some non-linear function determining how much ‘additional’ GQD is possible for each system size. We conjecture the form of this function by assuming an exponential fit, predicting

$$\xi(N) \simeq -0.3320e^{-0.2863N} + 0.2056 \quad (N > 1). \quad (17)$$

VI. CONCLUSIONS AND OUTLOOK

We have presented a protocol by which significant amounts of quantum correlations can be distributed to quantum memories through a classically correlated resource state. The amount of discord distributed depends only on the measurement basis, regardless of the measurement outcomes. We have also provided numerical evidence of scalability for a desired number of quantum memories, which may all share large amounts of discord. In addition, the robustness of the protocol has been evaluated, revealing an inherent robustness to imprecise measurement settings. Recent work has also shown that, with larger amounts of classical correlation in the resource state, it is also possible to generate other types of discordant states through local operations such as Werner states [19]. We explore how our protocol may be adapted for this possibility with a correlated noise channel applied to the memories in App. II.

In future work, one may consider how to use the distributed discord network in a practical way, and the protocol here is yet to stand up to experimental scrutiny. Moreover, the possibility of using weakly-entangled initial states to enable higher amounts of distributed discord can be explored. The true usefulness of a discord distribution scheme like the one detailed here remains to be seen, owing to the fact that discord may still have unexplored potential as a resource in quantum information processing, even if only as a vehicle for establishing entanglement. While discord is the resource for entanglement distribution, classical correlation is a resource for discord distribution.

The protocol proposed here is versed to implementation in at least two mainstream platforms, namely cavity quantum electrodynamics (QED) [42, 43] and its circuital version [44]. In both platforms, which have enjoyed significant success in demonstrating the power of measurement-enhanced coherent information processing [45–47], the carrier states could be encoded in the polarisation degree of freedom of radiation-based qubits (microwave signals in the case of circuit QED). The

memories, instead, would be encoded in neutral atoms trapped in optical cavities or superconducting transmon qubits embedded in stripline resonators. In both setups, the controlled- Z operations required can be realized from light-matter interactions formally describable in terms of the effective operations reported in Ref. [48], even if the probability of such operations failing nears unity [49]. This potential experimental setting would provide avenues for space-to-ground (or ground-to-ground) discord distribution, with recent work exploring zero-added loss photon sources [50]. Using our protocol, the quantum correlations themselves would not be subject to any noise that the photons are subject to when travelling from the source to the labs, since these correlations would be created locally from the labs. While this brings an advantage, one must be careful in ensuring that the classical correlations remain robust to the environment, and future works may consider the robustness of this protocol to noise models. We also consider this setup to be ideal for distributed quantum computation, since non-local (entangling) gates can be performed on two remote atoms trapped in different optical cavities [51].

The data generated as part of this work are available from Ref. [52] and, upon reasonable requests, from the authors.

ACKNOWLEDGMENTS

We acknowledge support by the European Union’s Horizon Europe EIC-Pathfinder project QuCoM (101046973), the Royal Society Wolfson Fellowship (RSWF/R3/183013), the UK EPSRC (EP/T028424/1), the Department for the Economy Northern Ireland under the US-Ireland R&D Partnership Programme, the “Italian National Quantum Science and Technology Institute (NQSTI)” (PE0000023) - SPOKE 2 through project ASpEQct, the “National Centre for HPC, Big Data and Quantum Computing (HPC)” (CN00000013) – SPOKE 10 through project HyQELM, and the EU Horizon Europe EIC Pathfinder project QuCoM (GA no. 10032223).

-
- [1] H. J. Kimble, The quantum internet, *Nature* **453**, 1023 (2008).
 - [2] S. Wehner, D. Elkouss, and R. Hanson, Quantum internet: A vision for the road ahead, *Science* **362**, eaam9288 (2018).
 - [3] H. Ollivier and W. H. Zurek, Quantum Discord: A Measure of the Quantumness of Correlations, *Phys. Rev. Lett.* **88**, 017901 (2001).
 - [4] L. Henderson and V. Vedral, Classical, quantum and total correlations, *J. Phys. A: Math. Gen.* **34**, 6899 (2001).
 - [5] A. Al-Qasimi and D. F. V. James, Comparison of the attempts of quantum discord and quantum entanglement to capture quantum correlations, *Phys. Rev. A* **83**, 032101 (2011).
 - [6] M. Piani, S. Gharibian, G. Adesso, J. Calsamiglia, P. Horodecki, and A. Winter, All Nonclassical Correlations Can Be Activated into Distillable Entanglement, *Phys. Rev. Lett.* **106**, 220403 (2011).
 - [7] S. Gharibian, M. Piani, G. Adesso, J. Calsamiglia, and P. Horodecki, Characterizing quantumness via entanglement creation, *Int. J. Quantum Inf.* **9**, 1701 (2011).
 - [8] A. Datta, A. Shaji, and C. M. Caves, Quantum Discord and the Power of One Qubit, *Phys. Rev. Lett.* **100**, 050502 (2008).

- [9] B. P. Lanyon, M. Barbieri, M. P. Almeida, and A. G. White, Experimental Quantum Computing without Entanglement, *Phys. Rev. Lett.* **101**, 200501 (2008).
- [10] B. Dakić, Y. O. Lipp, X. Ma, M. Ringbauer, S. Barz, T. Paterek, V. Vedral, A. Zeilinger, Č. Brukner, and P. Walther, Quantum discord as resource for remote state preparation, *Nat. Phys.* **8**, 666 (2012).
- [11] L. Roa, J. C. Retamal, and M. Alid-Vaccarezza, Dissonance is Required for Assisted Optimal State Discrimination, *Phys. Rev. Lett.* **107**, 080401 (2011).
- [12] B. Li, S.-M. Fei, Z.-X. Wang, and H. Fan, Assisted state discrimination without entanglement, *Phys. Rev. A* **85**, 022328 (2012).
- [13] C.-Q. Pang, F.-L. Zhang, L.-F. Xu, M.-L. Liang, and J.-L. Chen, Sequential state discrimination and requirement of quantum dissonance, *Phys. Rev. A* **88**, 052331 (2013).
- [14] F.-L. Zhang, J.-L. Chen, L.-C. Kwek, and V. Vedral, Requirement of dissonance in assisted optimal state discrimination, *Sci. Rep.* **3**, 2134 (2013).
- [15] S. Pirandola, Quantum discord as a resource for quantum cryptography, *Sci. Rep.* **4**, 6956 (2014).
- [16] R. Wang, G.-J. Fan-Yuan, Z.-Q. Yin, S. Wang, H.-W. Li, Y. Yao, W. Chen, G.-C. Guo, and Z.-F. Han, Secure Key from Quantum Discord, (2023), arXiv preprint, arXiv:2304.05880 [quant-ph].
- [17] A. Streltsov, H. Kampermann, and D. Bruß, Behavior of Quantum Correlations under Local Noise, *Phys. Rev. Lett.* **107**, 170502 (2011).
- [18] F. Ciccarello and V. Giovannetti, Creating quantum correlations through local nonunitary memoryless channels, *Phys. Rev. A* **85**, 010102(R) (2012).
- [19] G. Torun, Generating quantum dissonance via local operations, *Int. J. Quantum Inf.*, 2450044 (2024).
- [20] S. Campbell, T. J. G. Apollaro, C. Di Franco, L. Banchi, A. Cuccoli, R. Vaia, F. Plastina, and M. Paternostro, Propagation of nonclassical correlations across a quantum spin chain, *Phys. Rev. A* **84**, 052316 (2011).
- [21] F. Ciccarello and V. Giovannetti, Local-channel-induced rise of quantum correlations in continuous-variable systems, *Phys. Rev. A* **85**, 022108 (2012).
- [22] B. P. Lanyon, P. Jurcevic, C. Hempel, M. Gessner, V. Vedral, R. Blatt, and C. F. Roos, Experimental Generation of Quantum Discord via Noisy Processes, *Phys. Rev. Lett.* **111**, 100504 (2013).
- [23] T. S. Cubitt, F. Verstraete, W. Dür, and J. I. Cirac, Separable States Can Be Used To Distribute Entanglement, *Phys. Rev. Lett.* **91**, 037902 (2003).
- [24] A. Kay, Using Separable Bell-Diagonal States to Distribute Entanglement, *Phys. Rev. Lett.* **109**, 080503 (2012).
- [25] A. Laneve, H. McAleese, and M. Paternostro, A scheme for multipartite entanglement distribution via separable carriers, *New J. Phys.* **24**, 123003 (2022).
- [26] C. J. Campbell, A. G. Hawkins, G. Zicari, M. Paternostro, and H. McAleese, Entanglement distribution through separable states via a zero-added-loss photon multiplexing inspired protocol, *Phys. Rev. Res.* **6**, 033317 (2024).
- [27] A. Streltsov, H. Kampermann, and D. Bruß, Quantum Cost for Sending Entanglement, *Phys. Rev. Lett.* **108**, 250501 (2012).
- [28] T. K. Chuan, J. Maillard, K. Modi, T. Paterek, M. Paternostro, and M. Piani, Quantum Discord Bounds the Amount of Distributed Entanglement, *Phys. Rev. Lett.* **109**, 070501 (2012).
- [29] F. Galve, G. L. Giorgi, and R. Zambrini, Orthogonal measurements are almost sufficient for quantum discord of two qubits, *EPL* **96**, 40005 (2011).
- [30] K. Modi, A. Brodutch, H. Cable, T. Paterek, and V. Vedral, The classical-quantum boundary for correlations: Discord and related measures, *Rev. Mod. Phys.* **84**, 1655 (2012).
- [31] C. H. Bennett, Quantum cryptography using any two nonorthogonal states, *Phys. Rev. Lett.* **68**, 3121 (1992).
- [32] We use the term *in general* to remark that there exist certain carrier measurement bases, such as the computational one, whereby no discord is generated. The resulting state will still have the same structure as a classical-quantum state, but will not possess asymmetric discord. Therefore, the state, in general, has asymmetric discord. This reasoning is also applied to the rest of Sec. V in all instances where we refer to a state having discord *in general*.
- [33] For reference, the discord of a maximally entangled pure state of two qubits is exactly 1.
- [34] M. A. Nielsen and I. L. Chuang, *Quantum Computation and Quantum Information (10th Anniversary Edition)* (Cambridge University Press, 2010).
- [35] M. Curty, M. Lewenstein, and N. Lütkenhaus, Entanglement as a Precondition for Secure Quantum Key Distribution, *Phys. Rev. Lett.* **92**, 217903 (2004).
- [36] G. Carrara, H. Kampermann, D. Bruß, and G. Murta, Genuine multipartite entanglement is not a precondition for secure conference key agreement, *Phys. Rev. Res.* **3**, 013264 (2021).
- [37] C. C. Rulli and M. S. Sarandy, Global quantum discord in multipartite systems, *Phys. Rev. A* **84**, 042109 (2011).
- [38] V. Vedral, The role of relative entropy in quantum information theory, *Rev. Mod. Phys.* **74**, 197 (2002).
- [39] Higher-dimensional systems than 5 qubits were also attempted, however the simulations and optimizations were too computationally expensive.
- [40] W. Dür, G. Vidal, and J. I. Cirac, Three qubits can be entangled in two inequivalent ways, *Phys. Rev. A* **62**, 062314 (2000).
- [41] Unlike the bipartite case, some multipartite *pure* states – including $|W_3\rangle$ – may possess other quantum correlations in addition to entanglement, which have been dubbed *quantum dissonance* [53].
- [42] H. Walther, B. T. H. Varcoe, B.-G. Englert, and T. Becker, Cavity quantum electrodynamics, *Rep. Prog. Phys.* **69**, 1325 (2006).
- [43] C. Monroe, Quantum information processing with atoms and photons, *Nature* **416**, 238 (2002).
- [44] A. Blais, A. L. Grimsmo, S. M. Girvin, and A. Wallraff, Circuit quantum electrodynamics, *Rev. Mod. Phys.* **93**, 025005 (2021).
- [45] M. Mićuda, R. Stárek, J. Fiurášek, and R. Filip, Decoherence-Resilient Linear Optical Two-Qubit Quantum Gate, *Phys. Rev. App.* **14**, 054066 (2020).
- [46] R. Stárek, M. Mićuda, M. Kolář, R. Filip, and J. Fiurášek, Experimental demonstration of optimal probabilistic enhancement of quantum coherence, *Quantum Sci. Technol.* **6**, 045010 (2021).
- [47] G. L. Zanin, M. Antesberger, M. J. Jacquet, P. H. S. Ribeiro, L. A. Rozema, and P. Walther, Enhanced Photonic Maxwell’s Demon with Correlated Baths, *Quantum* **6**, 810 (2022).

- [48] L.-M. Duan and H. J. Kimble, Scalable Photonic Quantum Computation through Cavity-Assisted Interactions, *Phys. Rev. Lett.* **92**, 127902 (2004).
- [49] L.-M. Duan and R. Raussendorf, Efficient Quantum Computation with Probabilistic Quantum Gates, *Phys. Rev. Lett.* **95**, 080503 (2005).
- [50] K. C. Chen, P. Dhara, M. Heuck, Y. Lee, W. Dai, S. Guha, and D. Englund, Zero-Added-Loss Entangled-Photon Multiplexing for Ground- and Space-Based Quantum Networks, *Phys. Rev. Appl.* **19**, 054029 (2023).
- [51] L.-M. Duan, B. Wang, and H. J. Kimble, Robust quantum gates on neutral atoms with cavity-assisted photon scattering, *Phys. Rev. A* **72**, 032333 (2005).
- [52] <https://www.doi.org/10.5281/zenodo.13890507>.
- [53] K. Modi, T. Paterek, W. Son, V. Vedral, and M. Williamson, Unified View of Quantum and Classical Correlations, *Phys. Rev. Lett.* **104**, 080501 (2010).

APPENDIX I: CRITICAL ANALYSIS OF THE BIPARTITE PROTOCOL

It has been shown that the action of certain local quantum channels on bipartite states could generate discord [17, 18]. Examples of such a peculiar effect, which puts discord at variance with entanglement for which such a result is not possible, have been shown in Refs. [20–22]. The class of quantum channels that are able to generate discord locally are those that are neither *semiclassical* nor *unital*, as reported by Ref. [17].

A semiclassical channel Λ_{sc} is one that maps all input states ρ onto output ones $\Lambda_{\text{sc}}(\rho)$ that are diagonal in the same basis. When considered against the state achieved through our protocol applied to the to the initial state $\rho_{M_1 M_2}$, we see that the final state is diagonal in the $\{|++\rangle, |+-\rangle, |-+\rangle, |--\rangle\}$ basis only when $\theta_1 = \{0, \pi\}$ and/or $\theta_2 = \{0, \pi\}$ (i.e., when either carrier is measured in the computational basis). We have further found that these parameters will result in a semiclassical channel for any other classical input state of the memories. In all such instances, the resulting discord is zero. This is not implied if the initial state of the memories is discordant; rather, it is implied that the resulting *increase* of discord will always be zero. For all other values of $\theta_{1,2}$, the channel entailed by our protocol may, in general, not be semiclassical.

Meanwhile, a unital channel Λ_{un} is one that maps the maximally mixed state $\mathbb{1}/d$ of a d -dimensional system to itself, i.e.

$$\Lambda_{\text{un}}\left(\frac{1}{d}\mathbb{1}\right) = \frac{1}{d}\mathbb{1}. \quad (18)$$

When applied to the initial state $\rho_{M_1 M_2} = \frac{1}{4}\mathbb{1}$ of the memories, our protocol returns the measurement-dependent state

$$\rho_{M_1 M_2} = \frac{1}{4}\mathbb{1} + \frac{1}{4}(\cos\phi_1 \cos\phi_2 \sin\theta_1 \sin\theta_2)Z_{M_1} \oplus (-Z_{M_2}), \quad (19)$$

showing that, in general, the channel is not unital. However, the channel *is* unital for one (or a combination) of the following cases: $\theta_{1,2} = 0, \pi$ and $\phi_{1,2} = \pi/2, 3\pi/2$. Since the amount of discord is independent of the values of $\phi_{1,2}$, we see that we can generate the maximum amount of discord here even from a unital channel, for example with the parameters $\theta_1 = \pi/2$, $\theta_2 = \pi/4$, $\phi_1 = \pi/2$, $\phi_2 = 0$.

Despite the protocol resulting in a unital effective channel for the memories, our scheme is not in contradiction with the findings of Ref. [17] due to the initial state of the carriers. The (classical) correlations initially shared by C_1 and C_2 in Eq. (1) prevent the resulting quantum channel affecting the memories to be factorized, thus is not *mathematically local*. More formally, despite the local nature of the operations performed on the memories, the initial carrier correlations results in a channel $\Lambda_{M_1 M_2}(\rho_{M_1 M_2}) \neq \Lambda_{M_1}(\rho_{M_1}) \otimes \Lambda_{M_2}(\rho_{M_2})$ with $\rho_{M_j} = \text{Tr}_{k \neq j} \rho_{M_1 M_2} = |+\rangle\langle +|_{M_j}$ ($j, k = 1, 2$) in light of Eq. (1).

This point could be further corroborated by studying the performance of the protocol resulting from the use of just one memory, say M_2 , initially in state $|+\rangle_{M_2}$. A controlled- Z gate is applied to the joint state of C_2 and M_2 before C_2 is measured, while no action is taken on C_1 . In this case, any discord produced will be asymmetric and we generate classical-quantum states instead of quantum-quantum states. For $\theta_2 = \{\pi/4, 3\pi/4\}$, the corresponding state of the C_1 - M_2 compound carries the same amount of discord of 0.2018 found in the two-memory configuration. To test unitality, we act with this protocol on the initial state $\rho_{C_1 C_2} \otimes \mathbb{1}_{M_2}/2$, meaning the initial state of $C_1 M_2$ (as well as $C_2 M_2$) is maximally mixed. The corresponding final state of $C_1 M_2$ is $\mathbb{1}_{C_1 M_2}/4$ for one of the choices $\theta_2 = \{0, \pi\}$, $\phi_2 = \{\pi/2, 3\pi/2\}$ being satisfied. However, the amount of discord seeded in the state of such compounds is again independent of ϕ_2 , thus implying that the channel is discord-generating when unital, despite the locality of the considered operations. Nonetheless, we conclude that, since the initial state cannot be written as a tensor product of the form $\rho_{C_1 M_2} \otimes \rho_{C_2}$ due to the initial classical correlations between C_1 and C_2 , the statement in Ref. [17] again does not apply here.

APPENDIX II: PERFORMANCE OF THE BIPARTITE PROTOCOL UNDER CORRELATED DEPHASING NOISE

One of the motivations of our protocol is the ability to generate discord between two quantum memories via bi-local operations only, without and direct communication between said memories. With that being said, we also wish to explore how our protocol may perform under correlated noise being applied to the memories. We

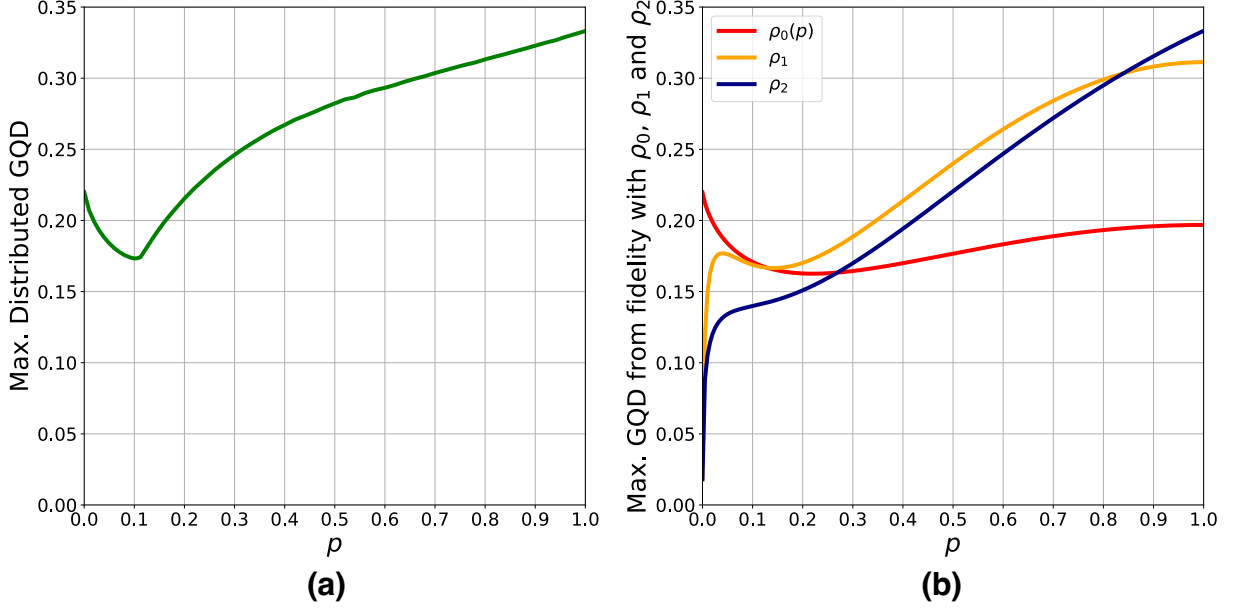


FIG. 6. **(a)** The amount of GQD in the final memory state, maximized over the carrier measurement parameters, plotted as a function of the strength p of a fully correlated dephasing channel acting on the initial state of the memories M_1 and M_2 . **(b)** GQD of $\rho_0(p)$ along with the maximum amount of GQD possible (as a result of the protocol) from fidelity with the states ρ_1 and ρ_2 , optimizing fidelity over carrier measurements.

model such noise using the following Kraus operators

$$K_1(p) = \sqrt{1 - \frac{p}{2}} (\mathbb{I}_{M_1} \otimes \mathbb{I}_{M_2}) \quad (20)$$

$$K_2(p, \mu) = \sqrt{\frac{p}{2}(1 - \mu)} (Z_{M_1} \otimes \mathbb{I}_{M_2}) \quad (21)$$

$$K_3(p, \mu) = \sqrt{\frac{p}{2}(1 - \mu)} (\mathbb{I}_{M_1} \otimes Z_{M_2}) \quad (22)$$

$$K_4(p, \mu) = \sqrt{\frac{p}{2}\mu} (Z_{M_1} \otimes Z_{M_2}), \quad (23)$$

characterized by the strength of the noise $0 \leq p \leq 1$ and the strength of the correlation $0 \leq \mu \leq 1$. We assume the extremal case $\mu = 1$ in order to assess the performance of the protocol with as much classical correlation in the initial $C_1M_1 : C_2M_2$ bipartition as possible. We compute the maximum GQD (with respect to the measurement parameters) for each value of p and display our results in Fig. 6 **(a)**. After an initial drop in the maximum amount of GQD, we actually find, rather counter-intuitively, that more GQD is possible under correlated dephasing noise for strengths $p \gtrsim 0.21$ than for when there is no noise at all, obtaining a maximum GQD of $\frac{1}{3}$. for $p = 1$. This rise in maximum GQD may not be completely unexpected, since this type of noise channel will increase the classical correlation in the previously-uncorrelated state. In fact, for $p = 1$ the state in Eq (1) is now also the initial state of the memories, meaning twice the initial classical correlations in $C_1M_1 : C_2M_2$. Nevertheless, what is especially peculiar about Fig. 6 **(a)** is the fall before the sudden rise at around $p \approx 0.11$.

To explain this behavior, we consider discordant states of different structures with which the final state of the memories may have a high fidelity with. Such states may include Werner states [19] and mixtures of Bell states, so we consider the following three types of discordant states:

1. For each p , the state resulting from the carrier measurement parameters being taken as the same used in the noiseless ($p = 0$) case, assuming $\theta_1 = \theta_2 = 0.9458$ and $\phi_1 = \phi_2 = 0$:

$$\rho_0(p) = \rho'_{M_1M_2}(p). \quad (24)$$

2. The following Bell state mixture:

$$\rho_1 = \frac{1}{2} |\Psi^+\rangle\langle\Psi^+| + \frac{1}{4} (|\Phi^+\rangle\langle\Phi^+| + |\Phi^-\rangle\langle\Phi^-|). \quad (25)$$

This state has a GQD of 0.3113 and is almost entangled; if it parameterised as

$$\tau(x) = x |\Psi^+\rangle\langle\Psi^+| + \frac{(1-x)}{2} (|\Phi^+\rangle\langle\Phi^+| + |\Phi^-\rangle\langle\Phi^-|) \quad (26)$$

with $x \in [0, 1]$, then it is entangled for $x > \frac{1}{2}$.

3. The following Bell state mixture:

$$\rho_2 = \frac{1}{3} (|\Psi^+\rangle\langle\Psi^+| + |\Phi^+\rangle\langle\Phi^+| + |\Phi^-\rangle\langle\Phi^-|). \quad (27)$$

This state is equivalent to $\tau(\frac{1}{3})$ and has a GQD of exactly $\frac{1}{3}$, so it is further from being an entangled state than $\tau(\frac{1}{2})$ despite being more discordant.

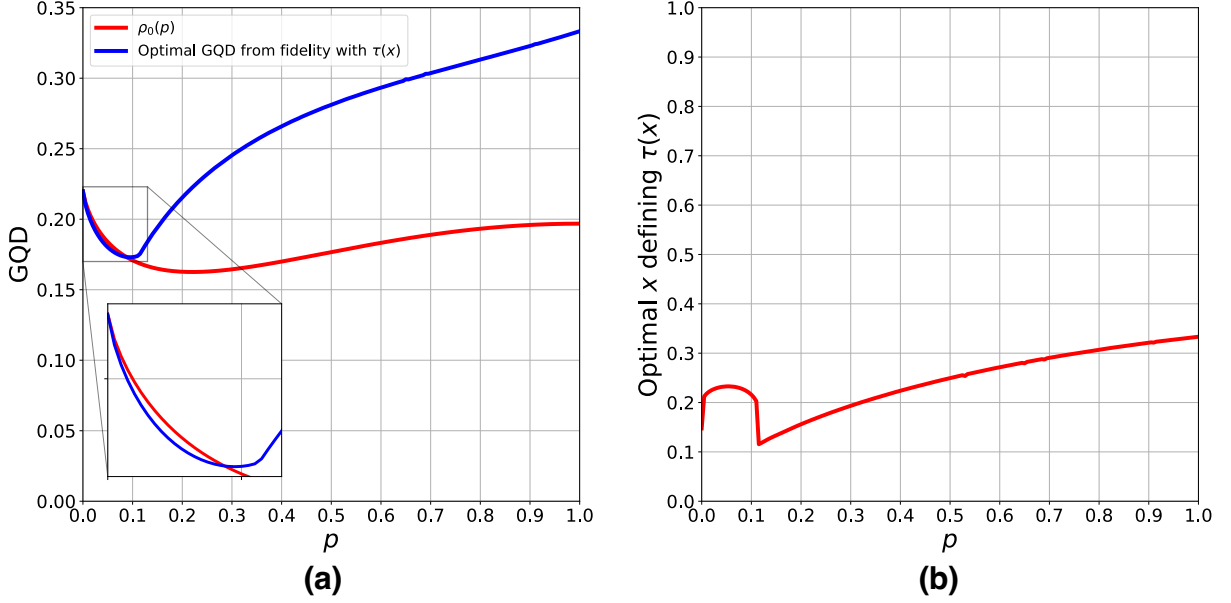


FIG. 7. **(a)** GQD of $\rho_0(p)$ along with the maximum amount of GQD possible (with respect to the carrier measurements) when searching the maximum fidelity values with the $\tau(x)$ states (with respect to x). A zoomed region is shown for $0 \leq p \leq 0.13$. **(b)** Optimal x values plotted against p . Each optimal x defines the state $\tau(x)$ with which a high fidelity results in the most GQD for each p -value.

For each p , we find $\mathcal{G}(\rho_0(p))$ as well as the GQD of the states which have the greatest fidelities with ρ_1 and ρ_2 . That is to say, we calculate $\max_{\theta_{1,2}, \phi_{1,2}} [\mathcal{F}(\rho'_{M_1 M_2}(p), \rho_i)]$ for $i = 1, 2$ and where $\mathcal{F}(\sigma_k, \sigma_l)$ denotes the fidelity between two quantum states σ_k and σ_l . Once the optimal measurement parameters are found by this maximization, we find the GQD of the corresponding state for each p . We plot our findings in Fig. 6 (b). If we look at the maximum value of the three plots for each value of p , the graph ends up looking remarkably similar to Fig. 6 (a), and so we may attribute the behavior to changing fidelities with Bell state mixtures for different values of p .

We also note that the optimal 'target state' (in terms of GQD) for $p = 1$ is ρ_2 , with a fidelity extremely close to 1 with this state when the measurement parameters $\theta_1 = \theta_2 \approx 0.9553$ and $\phi_1 = \phi_2 = 3\pi/4$ are used. However, one change in this modified protocol compared to the original is that the GQD is no longer measurement-outcome independent. For $p = 1$ and the measurement basis defined using the above angles, ρ_2 is only obtained with a fidelity close to unity when the measurement outcomes are identical, which occurs with probability $\frac{1}{2}$. If orthogonal measurement outcomes are observed, then the memories are left in a state that has a GQD of ~ 0.1258 corresponding to a very high fidelity with the Werner state $y|\Psi^-\rangle\langle\Psi^-| + \frac{1-y}{4}\mathbb{I}$ for $y = \frac{1}{3}$. We point out that this state is entangled for $y > \frac{1}{3}$.

Although this gives an idea as to why Fig. 6 (a) exhibits such peculiar behavior, we wish recreate it exactly

using the logic used to generate Fig. 6 (b). To do this, we assume that the 'target state' which with a high fidelity will give the maximum amount of GQD is of the form $\tau(x)$, but with a different x for each p . That is to say, each value of p has a different optimal value of x which defines the target state $\tau(x)$; this optimal value of x results in the maximum amount of GQD when the fidelity between the memory state and $\rho_3(x)$ is optimized over carrier measurements. It is not helpful to simply find the value of x which results in the maximum fidelity, as the maximum fidelity doesn't necessarily also result in the maximum GQD.

Employing an optimization algorithm incorporating a grid-search, we obtain the blue plot in Fig. 7 (a). This plot is almost identical to Fig. 6 (a) apart from $0 \leq p \lesssim 0.09$ in which there are smaller optimal values of GQD. In order to exactly recreate the results, we include the plot of GQD in the $\rho_0(p)$ states from Fig. 6 (b); taking the maximum between the two plots for each p results in a perfect copy of the original graph. This suggests that $p \approx 0.09$ is some 'threshold value' of correlated noise, beyond which fidelity with mixtures of Bell states outperforms the structure of states obtained from the original protocol. We visualize the sudden rise at $p \approx 0.12$ further by plotting the optimal value of x against p in Fig. 7 (b). One can see that the optimal 'target state' suddenly changes at this value of p , indicating that beyond this value, states close to $\tau(x)$ can both outperform $\rho_0(p)$ and keep increasing with the noise strength.